Structure of three-component microemulsions in the critical region determined by small-angle neutron scattering

Michael Kotlarchyk and Sow-Hsin Chen
Nuclear Engineering Department, Massachusetts Institute of Technology, Cambridge, Massachusetts 02139

John S. Huang and Mahn Won Kim
Exxon Research and Engineering Company, Annandale, New Jersey 08801
(Received 10 November 1983)

The intensity distribution of the critical scattering from sodium di-2-ethylhexylsulfosuccinate AOT—D_2O—*n*-alkane water-in-oil (W/O) microemulsions has been measured over an extensive range of droplet volume fractions (3—30 vol %) and temperatures (22 to 43 °C) in the critical region. The water/surfactant molar ratio of the microemulsion was kept at a constant value of 40.8, for which previous experiments on the temperature variation have been well documented. A structural model of W/O microemulsions based on well-defined surfactant-coated water droplets is firmly established up to a volume fraction of about 20 vol % for all temperatures studied. Data analysis assumes that the cloud points and subsequent phase separation are caused by concentration fluctuations of polydisperse droplets. The major conclusions drawn from the analysis are as follows. (1) The order parameter of the critical phenomenon can be taken to be the volume fraction of the dispersed droplets. (2) The size and polydispersity of the droplets remain essentially constant in the vicinity of the critical point (for a fixed water/surfactant ratio). (3) The critical phenomenon is driven by an increased attraction between the droplets as the critical point is approached. (4) The critical point can be approached by either raising the temperature at fixed volume fraction or by varying the carbon number of the oil solvent at fixed volume fraction and temperature. (5) The nature of the droplets does not change upon a phase separation into two coexisting microemulsions. The data also gives some evidence that the droplet picture of the microemulsion breaks down at sufficiently high concentrations of water and surfactant.

I. INTRODUCTION

A water-in-oil (W/O) microemulsion is a transparent liquid consisting of small droplets of water dispersed in a continuous phase of oil with the aid of a sufficient amount of surfactant and cosurfactant. The experimental determination of the detailed structure of microemulsion droplets in different phases is of primary importance in testing recent statistical thermodynamic theories of stability, phase behavior, and structure in these systems. The AOT-water-oil system (where AOT stands for sodium di-2-ethylhexylsulfosuccinate) is a particularly useful model system for measuring the characteristics of simple microemulsions since it forms one of the few three-component microemulsions in the vicinity of room temperature (i.e., no cosurfactant is needed). In addition, there are a wide range of compositions and temperatures that result in a single phase dispersion.

Most of the studies on microemulsion structure have been performed in the neighborhood of room temperature, where the temperature dependence of the microemulsion droplet structure is expected to be weak.[1–7] However, within the past few years, the existence of phase separation and critical behavior in the AOT-water-oil system has been observed as the temperature or the alkyl carbon number of the oil approach cloud points in certain areas of the phase diagram. Both quasielastic light scattering[8,9] and small-angle neutron scattering[10] (SANS) have shown a divergence of the correlation length and osmotic compressibility resembling the critical behavior of a binary liquid mixture. We have previously interpreted the increases in correlation length as being due to cluster formation of spherical droplets with a fixed size and polydispersity.

From the latter studies of the AOT-water-oil system, we have concluded that SANS is a powerful tool for determining structure in the critical region.[10] Although light scattering has been shown to be very useful for the study of critical fluctuations near the consolute point of binary liquid mixtures, it is nevertheless insufficient for the study of the structure of microemulsion phases. The primary reason is that the microemulsion droplets, at least far from the critical temperature T_c, have dimensions in the range of 50—100 Å. This size is not small in comparison to the correlation length ξ at the temperatures that have been studied. For instance, consider the case of a binary mixture of *n*-hexane and nitrobenzene. Chen *et al.*[11] reported that the correlation length varies with temperature along the critical isochore as $\xi=\xi_0\epsilon^{-\nu}$, where $\xi_0=3.64$ Å, $\nu=0.630$, and ϵ is the reduced temperature $\epsilon=|T_c-T|/T_c$. According to this relation, the correlation length, even at 28° away from T_c, has a value of $\xi=20$ Å, which is much larger than the molecular size of a few angstroms. Thus light scattering experiments always probe only one size ξ no matter what measurements, static or dynamic, are made. Specifically, a static scattering experiment measures the Ornstein-Zernike correlation

length ξ, while a dynamic experiment measures the effective diffusion coefficient $k_B T/6\pi\eta\xi$, where η is the solution viscosity. On the other hand, microemulsions present a different picture. For the AOT-water-decane system, the correlation length at 10° below T_c has been measured to be only about 132 Å, while the droplet diameter was determined to be about 100 Å.[10] The two lengths are indeed comparable for a wide range of temperatures of interest. Thus a dynamic light scattering experiment cannot really distinguish between the two lengths. This difficulty is further compounded by the fact that the mutual diffusion coefficient measured in a light scattering experiment is not simply related to the hydrodynamic radius of the droplets when strong interactions are present in the system. In order to be able to differentiate between the two lengths at each temperature, one must use an experimental technique having a wide range of wave-vector transfers Q capable of probing both the correlation length and the droplet diameter. SANS is just such a technique. Furthermore, it has added advantages in the case of the AOT-D_2O-oil system because (1) the microemulsion droplets appear like sharply contrasted pools of water in oil[12] and (2) the two-dimensional area detector used in SANS is easily calibrated to give an absolute scattering intensity. This is vital to the size and polydispersity analysis of a system of interacting particles, as we shall demonstrate shortly.

In the previous studies,[8–10] all measurements of critical behavior were performed along an isochore at the AOT-water-oil composition of 3-5-95, i.e., 3 g AOT and 5 cm^3 water in 95 cm^3 oil. This mixture is represented by point $D3$ shown on the ternary phase diagram (at $T=22.5$ °C) of the AOT-D_2O-decane system shown in Fig. 1. A systematic study of structure as a function of the composition and temperature in the vicinity of this point has not been undertaken with SANS primarily because such an investigation requires large amounts of SANS spectrometer time (which are usually difficult to obtain). Fortunately, during the past two years our group was able to obtain substantial beam time sufficient to proceed with, what we believe to be, the most comprehensive SANS investigation of the structure of the AOT-D_2O-oil system in the critical region. In particular, our investigation consisted of the following.

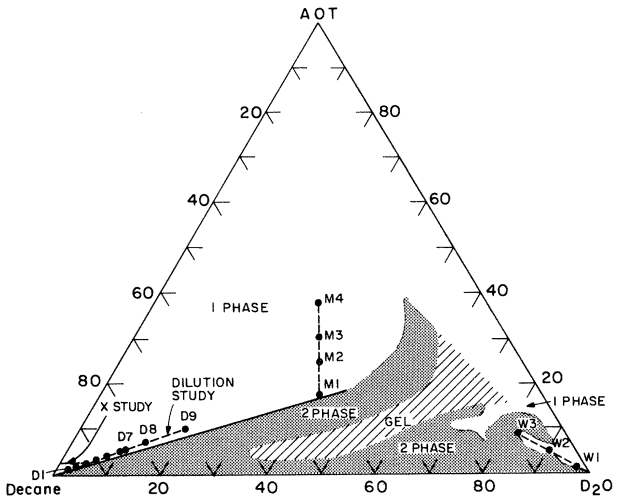

FIG. 1. Ternary phase diagram of AOT-D_2O-n-decane system at 22.5°C. Compositions are in volume percent. Points $D1$–$D9$ correspond to water-in-oil microemulsions investigated in the temperature and dilution study. An X study, where $X=[D_2O]/[AOT]$, was previously performed by Kotlarchyk, Chen, and Huang (Ref. 12). $W1$–$W3$ are oil-in-water dispersions and $M1$–$M4$ represent microemulsions with equal volumes of water and oil (to be presented in a future study).

(1) Temperature and dilution study—By maintaining the molar ratio $[D_2O]/[AOT]$ fixed at 40.8 and diluting with various amounts of n-decane containing 200 ppm of AOT, we were able to measure SANS spectra for the compositions represented by points $D1$–$D9$ in Fig. 1. These spectra were obtained for a series of temperatures between 22 °C and T_c (approximately 43 °C).

(2) Phase-separation study—SANS spectra were collected for both the upper and lower phases of a 3-5-95 phase-separated microemulsion to determine the structure and composition of the coexisting phases.

(3) Alkane-number study—SANS spectra were measured for a series of solvent carbon numbers at fixed temperature and composition in the critical region.

Before discussing these experiments, we shall give an outline of a general procedure used to interpret SANS spectra. In addition, a summary of our knowledge concerning the microscopic structure of individual droplets in microemulsions is presented.

II. INTERPRETATION OF SANS SPECTRA

The following is a general procedure for analyzing SANS spectra from interacting polydisperse spheres.[13] Consider the basic expression for the coherent scattering component of the differential cross section per unit volume given by the following ensemble average:

$$\frac{d\Sigma(\vec{Q})}{d\Omega}=V^{-1}\left\langle\left|\sum_{l=1}^{N} b_l \exp(i\vec{Q}\cdot\vec{r}_l)\right|^2\right\rangle . \tag{1}$$

Here, V is the sample volume, N is the number of nuclei in the sample, and b_l is the bound coherent scattering length of the lth nucleus. The position of the lth nucleus is denoted by $\vec{r}_l$ and $\vec{Q}$ is the scattering vector. In a SANS experiment, the magnitude of $\vec{Q}$ is equal to $(4\pi/\lambda)\sin(\theta/2)$, where λ is the wavelength of incident neutrons and θ is the scattering angle. Suppose the sample contains N_p spherical droplets immersed in a homogeneous solvent. Then one can imagine the sample volume to be partitioned into N_p cells, each containing exactly one droplet. Without losing any generality, the nuclei can be relabeled with two subscripts i and j as follows:

$$\frac{d\Sigma(\vec{Q})}{d\Omega}=V^{-1}\left\langle\left|\sum_{i=1}^{N_p}\sum_{j=1}^{N_i} b_{ij} \exp(i\vec{Q}\cdot\vec{r}_{ij})\right|^2\right\rangle , \tag{2}$$

where b_{ij} and $\vec{r}_{ij}$ are the scattering length and position of the jth nucleus contained in the ith cell. N_i is the number of nuclei in the ith cell. Denoting the center of droplet i

by $\vec{R}_i$ and the position of a nucleus at $\vec{r}_{ij}$ relative to this point by $\vec{X}_j$, one can make the decomposition $\vec{r}_{ij}=\vec{R}_i+\vec{X}_j$. Then,

$$\frac{d\Sigma(\vec{Q})}{d\Omega}=V^{-1}\left\langle\left|\sum_{i=1}^{N_p}\exp(i\vec{Q}\cdot\vec{R}_i)\times\sum_{j=1}^{N_i}b_{ij}\exp(i\vec{Q}\cdot\vec{X}_j)\right|^2\right\rangle . \quad (3)$$

Now define the form factor $F_i(\vec{Q})$ of the ith droplet as

$$F_i(\vec{Q})=\sum_{j=1}^{N_i}b_{ij}\exp(i\vec{Q}\cdot\vec{X}_j) . \quad (4)$$

Then,

$$\frac{d\Sigma(\vec{Q})}{d\Omega}=V^{-1}\left\langle\sum_{i=1}^{N_p}\sum_{i'=1}^{N_p}F_i(\vec{Q})F_{i'}^{*}(\vec{Q})\times\exp[i\vec{Q}\cdot(\vec{R}_i-\vec{R}_{i'})]\right\rangle . \quad (5)$$

The form factor $F_i(\vec{Q})$ is expressed in terms of the individual scattering lengths of the nuclei in the cell containing the ith droplet. For our case, it is more convenient to express the form factor in terms of scattering-length densities, thus rewriting Eq. (4) as

$$F_i(\vec{Q})=\int_{\text{cell}\,i}d\vec{r}\,\rho_i(\vec{r})\exp(i\vec{Q}\cdot\vec{r}) , \quad (6)$$

where

$$\rho_i(\vec{r})\equiv\sum_{j=1}^{N_i}b_{ij}\delta(\vec{r}-\vec{X}_j) \quad (7)$$

is the scattering-length density at position $\vec{r}$ of the ith cell. It is preferable to transform the form factor to an integral over the droplet volume only. Then Eq. (6) can be reexpressed as

$$F_i(\vec{Q})=\int_{\text{droplet}\,i}d\vec{r}\,[\rho_i(\vec{r})-\rho_s]\exp(i\vec{Q}\cdot\vec{r})+\rho_s\int_{\text{cell}\,i}d\vec{r}\exp(i\vec{Q}\cdot\vec{r}) , \quad (8)$$

where ρ_s is the scattering-length density of the solvent. Since the second integral is simply a δ function centered at $\vec{Q}=0$, we obtain

$$F_i(\vec{Q})=\int_{\text{droplet}\,i}d\vec{r}\,[\rho_i(\vec{r})-\rho_s]\times\exp(i\vec{Q}\cdot\vec{r}),\ \vec{Q}\neq 0 . \quad (9)$$

This is a standard result used extensively in SANS literature.[14] For a homogeneous spherical droplet of radius R, the above integration can be carried out to give

$$F_i(\vec{Q})=F_i(QR)=(4\pi/3)R^3\Delta\rho[3j_1(QR)/QR] , \quad (10)$$

where $\Delta\rho$ is the difference between the scattering-length density of the droplet and the solvent and $j_1(x)$ is the first-order spherical Bessel function.

Up to this point, the derivation of the scattering cross section has been completely general for spherical droplets. When considering droplets which are polydisperse, the form factor varies from droplet to droplet. At this point we make the approximation that droplet size is only weakly correlated to droplet position. In that case, we can write

$$\frac{d\Sigma(\vec{Q})}{d\Omega}=V^{-1}\left\langle\sum_{i=1}^{N_p}\sum_{i'=1}^{N_p}\langle F_i(\vec{Q})F_{i'}^{*}(\vec{Q})\rangle\times\exp[i\vec{Q}\cdot(\vec{R}_i-\vec{R}_{i'})]\right\rangle , \quad (11)$$

where the small angular bracket represents an average weighted by the distribution of droplet sizes. This average can be decomposed into

$$\langle F_i(\vec{Q})F_{i'}^{*}(\vec{Q})\rangle=[\langle|F(\vec{Q})|^2\rangle-|\langle F(\vec{Q})\rangle|^2]\delta_{ii'}+|\langle F(\vec{Q})\rangle|^2 . \quad (12)$$

Then the cross section reduces to

$$\frac{d\Sigma(\vec{Q})}{d\Omega}=n_p[\langle|F(\vec{Q})|^2\rangle-|\langle F(\vec{Q})\rangle|^2]+n_p|\langle F(\vec{Q})\rangle|^2S(\vec{Q}) , \quad (13)$$

where $n_p=N_p/V$ is the average number density of droplets in the sample and $S(\vec{Q})$ is the average interparticle structure factor defined by

$$S(\vec{Q})=N_p^{-1}\left\langle\sum_{i=1}^{N_p}\sum_{i'=1}^{N_p}\exp[i\vec{Q}\cdot(\vec{R}_i-\vec{R}_{i'})]\right\rangle . \quad (14)$$

Strictly speaking, when investigating a polydisperse system, one should deal with partial structure factors $S_{ij}(\vec{Q})$, determined by solving the matrix form of the Ornstein-Zernike equation for the pair potential U_{ij} between particles with hard-core diameters σ_i and σ_j. By assuming that droplet size and position are uncorrelated, one is forced to deal with the average structure factor $S(\vec{Q})$ of Eq. (14). Using representative examples we have previously shown[13] that it is reasonable to approximate $S(\vec{Q})$ with a structure factor calculated from the one-component Ornstein-Zernike equation using an effective potential with a physically reasonable value for the hard-core diameter σ.

To observe the effects of polydispersity on the scattering cross section, it is best to rewrite Eq. (13) as

$$\frac{d\Sigma(\vec{Q})}{d\Omega}=n_pP(\vec{Q})S'(\vec{Q}) , \quad (15)$$

by defining the terms

$$P(\vec{Q})=\langle|F(\vec{Q})|^2\rangle , \quad (16)$$

$$S'(\vec{Q})=1+\beta(\vec{Q})[S(\vec{Q})-1] , \quad (17)$$

$$\beta(\vec{Q})=|\langle F(\vec{Q})\rangle|^2/\langle|F(\vec{Q})|^2\rangle . \quad (18)$$

$S'(\vec{Q})$ acts as an apparent interparticle structure factor. β is a Q-dependent factor between zero and one that suppresses the oscillations of the average structure factor

$S(\vec{Q})$ in the observed scattering spectrum from a polydisperse system.

For the case of a system of polydisperse homogeneous spheres, the following expressions can be used to calculate the averages necessary for computing the scattering cross-section:

$$\langle |F(Q)|^2 \rangle = \int_0^\infty |F(QR)|^2 f(R) dR \ , \tag{19}$$

$$|\langle F(Q) \rangle|^2 = \left| \int_0^\infty F(QR) f(R) dR \right|^2 . \tag{20}$$

$f(R)dR$ is the probability of a sphere having a radius between R and $R+dR$. The above integrals can be computed analytically for a Schultz size distribution,[13] i.e., the case where $f(R)$ is given by the following expression:

$$f(R) = \left[\frac{z+1}{\bar{R}} \right]^{z+1} R^z \exp\left[-\left[\frac{z+1}{\bar{R}} R \right] \right] \frac{1}{\Gamma(z+1)} \ , \quad z > -1 \ , \tag{21}$$

where $\bar{R}$ is the mean of the distribution and z is a width parameter. $\Gamma(x)$ is the gamma function. The Schultz distribution is skewed toward larger sizes, tending to a Gaussian form at large values of z. The distribution approaches a δ function at $R=\bar{R}$ as z approaches infinity. Our previous study[13] on the effects of polydispersity on the apparent structure factor indicate that the detailed shape of the particle-size distribution is not crucial for determining the effects of low to moderate polydispersity. The polydispersity index $p=\sigma_R/\bar{R}$, where σ_R is the root-mean-square deviation from the mean size, is the primary determinant of the rather complicated function $\beta(Q)$, and thus of $S'(Q)$. Since the jth moment of the Schultz distribution is easily calculated by

$$\langle R^j \rangle = \frac{\Gamma(z+j+1)}{\Gamma(z+1)} \left[\frac{\bar{R}}{z+1} \right]^j , \tag{22}$$

the parameter p is simply

$$p = (\overline{R^2} - \bar{R}^2)^{1/2} / \bar{R} = (z+1)^{-1/2} . \tag{23}$$

The results of this section will be used in the subsequent analysis of the critical scattering data.

III. UNDERLYING PARTICLE STRUCTURE IN AOT-WATER-OIL MICROEMULSIONS

It is important to discuss the microscopic structure of W/O microemulsion droplets before considering the experiments on the critical phenomenon. Light scattering works of Day *et al.*[3] and Zulauf and Eicke[4] have established a picture of AOT W/O microemulsions consisting of spherical water cores, each coated by a monolayer of AOT, immersed in a continuous oil phase. SANS studies by Cabos and Delord[2] and Kotlarchyk, Chen, and Huang,[12] along with small-angle x-ray scattering measurements performed by Assih *et al.*,[15] confirm this picture of an inverse micelle with a water core.

An important issue to address, however, is whether any appreciable polydispersity is associated with the droplets. In a SANS study, where contrast is determined by differences in scattering-length density, neutrons are unable to distinguish the difference between the surfactant tails and the oil solvent because the chemical structures are so similar. As a result, if one prepares the microemulsion with D_2O instead of H_2O, SANS should essentially see a system of water droplets in a continuous background of oil. Analysis of the scattering pattern from such a system of spheres is particularly simple if one assumes that water penetrates into the entire head-group region. This latter picture is consistent with findings in the case of normal lithium dodecyl sulfate micelles in aqueous solution as determined by Bendedouch, Chen, and Koehler.[16]

Let us define the following parameters: R is the radius of the water core, V_W is the volume of D_2O in a core, V_{HT} is the total head-group volume in a microemulsion droplet, v_W is the specific volume of a D_2O molecule, v_H is the average volume occupied by a single head group, A_M is the average surface area of the core, and a_H is the average surface area occupied by a surfactant head group. Volume conservation requires that

$$(4\pi/3)\langle R^3 \rangle = V_W + V_{HT} \ . \tag{24}$$

By dividing both sides of Eq. (24) by

$$A_M = 4\pi \langle R^2 \rangle \ , \tag{25}$$

one obtains

$$\tfrac{1}{3}\langle R^3 \rangle / \langle R^2 \rangle = \frac{V_W}{A_M} + \frac{V_{HT}}{A_M} \ . \tag{26}$$

Now, note the relations

$$\frac{V_{HT}}{A_M} = \frac{v_H}{a_H} \tag{27}$$

and

$$\frac{V_W}{A_M} = \frac{v_W}{a_H} X \ , \tag{28}$$

where X is equal to the molar ratio $[D_2O]/[AOT]$. In addition, observe that $\langle R^3 \rangle / \langle R^2 \rangle$ depends on the polydispersity index $p=\sigma_R/\bar{R}$:

$$\langle R^3 \rangle / \langle R^2 \rangle = \alpha(p) \bar{R} \ , \tag{29}$$

where $\bar{R}$ is the mean of the polydispersity distribution function and $\alpha(p)$ depends on the particular functional form of the distribution. Then, Eq. (26) can be rewritten as

$$\alpha(p)\bar{R} = \frac{3v_W}{a_H} X + \frac{3v_H}{a_H} \ . \tag{30}$$

Using Eq. (22), $\alpha(p)$ for a Schultz distribution is

$$\alpha(p) = 1 + 2p^2 \ . \tag{31}$$

If a Gaussian distribution function is assumed, as was the case when a SANS determination of the droplet structure was previously performed,[12] then

$$\alpha(p) = \frac{1+3p^2}{1+p^2} \ . \tag{32}$$

However, for all the spectra analyzed, p was less than 0.35, which means that the discrepancy between the values of $\alpha(p)$ calculated from Eqs. (31) and (32) is at most about 2%. So it appears that the value of $\alpha(p)$ does not depend strongly on the precise functional form of the distribution function.

Equation (30) shows that if one measures the average water core radius $\bar{R}$ as a function of the molar ratio X, one should get a straight-line relationship, assuming that the polydispersity p is only a function of temperature, but not a function of X. This latter condition is indeed satisfied according to our previous study.[12] The straight line will have a slope which depends on the average head-group area a_H and a zero intercept which depends on the average head-group volume v_H, assuming that the specific volume of a water molecule in the core is that of bulk water.

Kotlarchyk, Chen, and Huang[12] have experimentally demonstrated that Eq. (30) is valid for the range of temperatures from $T=25$ to 33 °C, and for X from 8 to 50 (as represented by the X study shown in Fig. 1). With SANS data, the polydispersity analysis we described in Sec. II was used to obtain both p and $\bar{R}$. It was assumed that the solution was sufficiently dilute and the temperature was sufficiently far away from the critical point that the approximation $S(Q)=1$ was valid for the Q range measured. With the use of the bulk value of $v_W=30.15$ Å^3 for D_2O near room temperature, a determination of the head-group area gives $a_H \cong 62.5$Å^2 near room temperature. This value is in agreement with results of light scattering measurements.[3,4] It is worth remarking that the method described allows a straightforward way of determining a_H at a given temperature (and salt content) of the microemulsion droplet.

In a later section, it will be shown that the thickness of the surfactant-tail layer δ can be computed by incorporating an attractive interdroplet potential into the model. We can thus quantitatively establish the microscopic structure of the microemulsion droplets from a SANS experiment. It should be noted that, in the regime far away from the cloud point, dynamic light scattering measurements[3,4] generally indicate a system of monodisperse spheres with a hydrodynamic radius similar to what we obtain for $\bar{R}+\delta$. It is clear that SANS, even in the dilute regime, is superior in its sensitivity to polydispersity because the data covers a wide Q range and the intensity can be determined on an absolute scale. The section that follows describes experiments for measuring microemulsion structure in the critical regime.

IV. EXPERIMENTS

A. Samples

Each three-component microemulsion consisted of sodium di-2-ethylhexylsulfosuccinate (AOT) and heavy water dissolved in a normal alkane. The AOT surfactant was supplied by American Cyanimid and Fluka and the n-alkanes were a 99% + gold label product from Aldrich Chemical Co. The heavy water contained 99.96% D_2O and 0.04% H_2O.

Purification of the AOT was accomplished as follows. One part AOT dissolved in three parts methanol was passed through a 0.2-μm filter and dried *in vacuo* at 60 °C two times. One part of the resultant AOT and one part active charcoal dissolved in three parts hexane was then filtered and dried. High-pressure liquid chromatography performed before and after these steps indicate that the procedure is indeed effective. It should be realized, however, that trace amounts of water tend to remain in the AOT (roughly one H_2O molecule per AOT molecule).

Since AOT is known to undergo hydrolysis and form ethyl-hexyl-alcohol, chromatography was used to measure the amounts of this alcohol in our samples at various storage times. It was found that after 7 days there were 300 ppm of alcohol in our samples containing 3% (wt./vol.) AOT. The alcohol level increased slightly to 500 ppm after 6 months and remained unchanged after 2 years. One 4-year-old sample made with H_2O (instead of D_2O, as in the first three samples) showed an alcohol level of over 900 ppm. Our experiments were performed within 7 days after sample preparation.

A temperature and dilution study was performed with various samples derived from an original stock (batch A) of 6 g AOT + 10 cm^3 D_2O + 56.7 cm^3 n-decane, as represented by the composition $D8$ in Figs. 1 and 2. By progressively diluting with known volumes of 200 ppm AOT (Ref. 17) in n-decane, points $D1$, $D2$, and $D4$—$D8$ were prepared for SANS measurements at the series of temperatures indicated by open circles in Fig. 2. The vari-

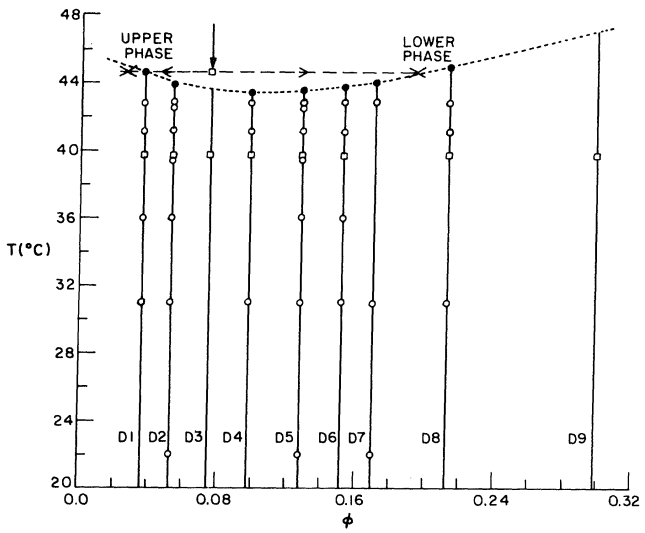

FIG. 2. Coexistence curve (solid points and dashed curve) for AOT—D_2O—n-decane microemulsions with molar ratio $[D_2O]/[AOT]=40.8$ containing batch A surfactant. (Microemulsions with batch B surfactant exhibit cloud points at about 2° lower than those with batch A surfactant.) Open circles represent volume fractions ϕ and temperatures T at which microemulsions containing batch A surfactant are measured during the temperature and dilution study. Open squares are points measured using microemulsions with batch B surfactant. The large crosses denote the concentrations of upper and lower phases resulting from a $\phi=0.0746$ microemulsion heated to about 1° above its cloud point (denoted by vertical arrow).

ous microemulsions were labeled by the volume fraction ϕ of the minor components as determined by the relation

$$\phi=\phi_{D_2O}+\phi_{AOT}\ , \tag{33}$$

where ϕ_{D_2O} and ϕ_{AOT} are the respective volume fractions of the heavy water and surfactant in the solution. The volume of AOT is assumed to be given by dividing the known weight of AOT by the density of dry surfactant (1.13 g/cm^3).[18] For this study the volume ratio ϕ/ϕ_{D_2O} and the molar ratio [D_2O]/[AOT] remained fixed at 1.531 and 40.8, respectively. A second set of microemulsions was prepared from a different stock (batch *B*) of AOT and measured with SANS only at 39.7 °C (open squares in Fig. 2). The apparent cloud point for this set was observed to be about 2° lower than that of the first. In addition to the previous compositions, this set included point *D* 3, which corresponds to the 3-5-95 system previously studied, and point *D* 9 which is much more concentrated than any of the other microemulsions in this dilution study.

A phase-separated system was prepared by heating the *D* 3 microemulsion in an external bath to 1° above the apparent cloud point and allowing approximately 24 h for the two phases to equilibrate. After measuring the volume occupied by each phase, an individual sample was prepared from each microemulsion by carefully pipetting a sufficient amount of the upper and lower phases to fill a scattering cell.

A set of $\phi=0.10$ microemulsions was prepared from yet another batch (batch *C*) of AOT in order to do an alkane-number study of critical behavior. By mixing known proportions of pure alkanes, the mean alkane number N_a of the microemulsion oil component was varied.

Each sample prepared was enclosed in a 1-mm pathlength cylindrical reentrant cell with 1-mm-thick quartz windows. During SANS measurements, temperature was controlled to within ± 0.1 °C of the desired temperature with a solid-state sensor.

B. SANS measurements

The experiments were conducted at the National Center for Small-Angle Scattering Research (NCSASR) at the Oak Ridge National Laboratory. The incident neutron wavelength of $\lambda=4.75$ Å ($\Delta\lambda/\lambda\cong 0.06$) was derived from the High Flux Isotope Reactor by passing the beam through a bank of graphite monochromating crystals followed by a cold beryllium filter. A 64×64 element two-dimensional position-sensitive proportional counter with a pixel size of 0.5×0.5 cm^2 was used for neutron detection. The spectrometer had a pinhole geometry with a 0.9-cm sample slit and either a 1.0- or 3.5-cm monochromator slit, for large and small sample-to-detector distances, respectively. The distance between the two pinholes was 7.6 m. With the 1.0 monochromator slit, the flux at the sample was about 3.5×10^4 neutrons/cm^2 sec.

The measured transmission of all samples was close to 52%. Most of the attenuation is from incoherent scattering due to the high hydrogen content of the *n*-alkane solvents, and it can be shown that multiple scattering effects are negligible for the coherent component of the spectra (see Appendix).

Two sets of intensity data were collected for each sample and temperature. One set was measured with a sample-to-detector distance (SDD) of 1310 cm, providing a Q range of about 4×10^{-3}–4×10^{-2} Å^{-1}. The counting times ranged from about 30 min for samples at high concentration and temperature to about 5 h for samples at low concentration and temperature. The second data set was measured with an SDD of 210 cm for a Q range of about 2.5×10^{-2}–2.5×10^{-1} Å^{-1}. For this distance, the counting times ranged between 15 min and 1 h. At each distance, scattering from pure *n*-alkane samples was used both to calibrate spatial nonuniformity of the detector sensitivity and to determine incoherent solvent scattering. After correcting the two-dimensional data sets for sensitivity, transmission, solvent scattering, and background, an on-line computer performed a radial average of the data arrays, giving values of the relative scattering intensity versus Q. Finally, the intensity spectra were converted to an absolute scale in units of probability of scattering per unit path length per unit solid angle $d\Sigma/d\Omega$(cm^{-1}). For a given spectrometer geometry, this was accomplished by measuring the scattering spectrum from a standard calibration sample with a well-known $d\Sigma/d\Omega$, such as aluminum (with a well-characterized void distribution) or water. At this point, the two spectra for a given sample were spliced to yield a single continuous scattering pattern covering a Q range from 4×10^{-3} to 0.25 Å^{-1}. The finite experimental resolution in Q space, $\langle \delta Q^2\rangle^{1/2}$, was calculated from the spectrometer geometry to be about 9×10^{-4} Å^{-1} for SDD equal to 1310 cm, and 4×10^{-3} Å^{-1} for SDD equal to 210 cm. This finite spread in Q is not expected to affect the size parameters of the droplet in an appreciable way. The measured correlation lengths and osmotic compressibilities can be affected by as much as 10%; however, the concentration and temperature dependence of these quantities is not significantly altered. The total collection time for data used in this and the previous study of structure in the critical region was approximately 20 days.

V. MODELS OF THE CRITICAL FLUCTUATIONS

To examine the critical behavior of the microemulsions it was assumed that scattering was caused by scattering-length density fluctuations of polydisperse spheres. The Q dependence of the scattered neutron intensity is modeled with Eqs. (15)–(18) by assuming a Schultz size distribution. Attempts were made to fit scattering data using two different models for the structure factor $S(Q)$.

In the first model, the following form for the structure factor is assumed:

$$S(Q)=1+\chi_T(1+Q^2\xi^2)^{-1}\ . \tag{34}$$

This form assumes an asymptotic Ornstein-Zernike (OZ) form[19] for the critical scattering at small Q, where ξ, the correlation length of the critical fluctuations, and χ_T, the isothermal susceptibility, both depend on the microemulsion volume fraction ϕ, temperature T, and alkane number N_a. The added factor of unity takes into account the

proper large-Q behavior of the structure factor for a system of finite-size particles. This structure factor, along with the relation for the droplet number density

$$n_p=\phi_{D_2O}\Big/\frac{4\pi}{3}\langle R^3\rangle$$
$$=\phi_{D_2O}\frac{(z+1)^2}{(z+2)(z+3)}\Big/\frac{4\pi}{3}\bar{R}^3\,, \tag{35}$$

is then used in our procedure for analyzing strongly interacting polydisperse spheres. Thus the five fitting parameters $\bar{R}$, z, $\Delta\rho$, ξ, and χ_T are required. In addition, a residual incoherent background term B and a parameter P, which splices the small- and large-Q spectra, were incorporated. The final values of the fitted parameters appear to be unique and the fittings always show that B is negligibly small and P is very close to unity.

The OZ structure factor provides an excellent model for the small-Q scattering in the critical regime where $\chi_T \gg 1$. In that case there is a rigorous limit:

$$\lim_{Q\to 0} S(Q)=n_p k_B T K_T=1+\chi_T\simeq\chi_T\,, \tag{36}$$

where K_T is the osmotic isothermal compressibility. Upon moving away from the critical point, however, one would expect Eq. (34) to gradually lose its validity since the OZ form no longer suffices. This anticipated deficiency of the OZ model occurs in the intermediate-Q region where one expects the interparticle structure factor $S(Q)$ to deviate from unity in an oscillatory fashion because well-defined neighbor shells exist in a dense fluid. In order to remedy these problems not too near the critical point, one needs to apply a microscopic theory of liquids.

In our second model for $S(Q)$ we assume that the spheres interact through an interparticle potential function taken to be a hard core of range σ plus an attractive Yukawa tail:

$$U(x)/k_BT=\begin{cases}-\gamma\exp(-kx)/x\,, & x\geq 1\\ \infty\,, & x<1\,,\end{cases} \tag{37}$$

where $x=r/\sigma$, and r is the interparticle separation. The range of the attractive tail is given by σ/k and the contact potential is $-\gamma\exp(-k)$, where $\gamma>0$.

In principle, one can calculate the structure factor $S(Q)$ by solving the Ornstein-Zernike equation for the net correlation function $h(x)$,

$$h(x)=c(x)+n_p\sigma^3\int h(|\vec{x}-\vec{x}'|)c(x')d\vec{x}' \tag{38}$$

and taking a Fourier transform,

$$S(Q)=1+4\pi n_p\sigma^3\int_0^\infty h(x)\frac{\sin(Q\sigma x)}{Q\sigma x}x^2dx\,. \tag{39}$$

One way to solve Eq. (38) is to make a mean spherical approximation (MSA) ansatz,[20] i.e.,

$$h(x)=-1 \quad \text{for } x<1 \tag{40}$$

$$c(x)=-U(x)/k_BT \quad \text{for } x>1\,. \tag{41}$$

The validity of this approximation for colloidal suspensions has been discussed by Hansen and Hayter[21] for a repulsive potential where $\gamma<0$. Furthermore, the MSA for an attractive potential has been successfully applied to the analysis of critical scattering from nonionic micelles.[22] That work indicates that the MSA should be valid for an attractive potential when the system is not too close to a critical point. In addition, an analytical solution using the potential function defined by Eq. (37) was given by Hayter and Penfold,[23] and a computer code written in FORTRAN exists for its convenient application. With the use of this program to calculate $S(Q)$, the fitting parameters for the scattering intensity are $\bar{R}$, z, $\Delta\rho$, k, and $\gamma\exp(-k)$. This assumes that the hard-sphere volume fraction ϕ_{HS} and the hard-sphere diameter σ are specified. In our model we postulated that $\phi_{HS}=\phi$. During the fitting procedure, the hard-sphere diameter was constrained by the relation

$$\sigma=(6\phi/\pi n_p)^{1/3}$$
$$=2(\phi/\phi_{D_2O})^{1/3}\langle R^3\rangle^{1/3}\,, \tag{42}$$

where n_p was calculated with Eq. (35).

The advantage of using the MSA is that one can extract the microscopic quantities σ, k, and γe^{-k}, which provide insight into the mechanisms of the critical behavior. Furthermore, the thickness δ of the surfactant-tail layer can be estimated from

$$\delta=\frac{\sigma}{2}-\langle R^3\rangle^{1/3}=[(\phi/\phi_{D_2O})^{1/3}-1]\langle R^3\rangle^{1/3}\,. \tag{43}$$

VI. RESULTS AND DISCUSSION

A. Temperature and dilution study

Figures 3 and 4 show the scattered neutron intensities for the dilution series at 39.7 °C (i.e., the open squares in Fig. 2), along with the fitted curves obtained by assuming the OZ model for $S(Q)$. The microemulsions in this series contained batch B surfactant, and these measurements were performed less than 1° below the critical temperature. The quality of the agreement between the fitted curves and data is typical of all temperatures investigated. The goodness of fit is very good ($\chi^2<3$) up to a volume fraction of about $\phi=0.13$, but it gradually degrades above this value. At $\phi=0.298$, attempts to use the OZ model fail completely, indicating either the use of an inadequate model for the structure factor or the breakdown of the spherical droplet picture of the microemulsion.

To illustrate the Q dependence of the various components contributing to a typical spectrum, Fig. 5 shows $P(Q)$, $S(Q)$, and $S'(Q)$ for the case of $\phi=0.0746$ shown in Fig. 3. Because of polydispersity, there is a considerable difference between the OZ structure factor $S(Q)$ and the apparent structure factor $S'(Q)$. It has been determined that the omission of the polydispersity parameter z causes significant degradation in the quality of the fit for this set of data.

The temperature and concentration dependence of the three droplet parameters $\Delta\rho$, $\bar{R}$, and p are graphed in Fig. 6. $\Delta\rho$ is seen to be fairly independent of ϕ and T. The average value of about 6.3×10^{-6} Å^{-2} is very close to the difference in scattering-length density between pure D_2O and n-decane (i.e., 6.8×10^{-6} Å^{-2}). It is certain that we

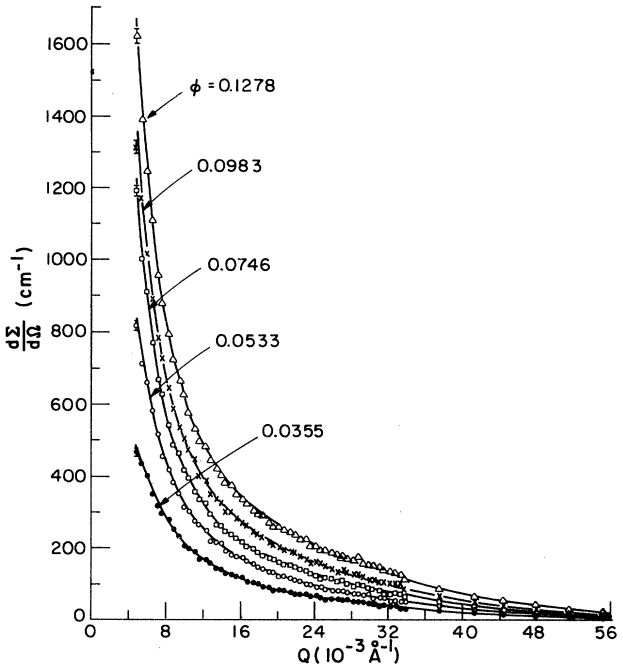

FIG. 3. SANS spectra at 39.7 °C for five volume fractions ϕ: 0.0355 (●), 0.0533 (○), 0.0746 (□), 0.0983 (×), 0.1278 (△). The solid curves represent best fits to data using OZ model for the structure factor.

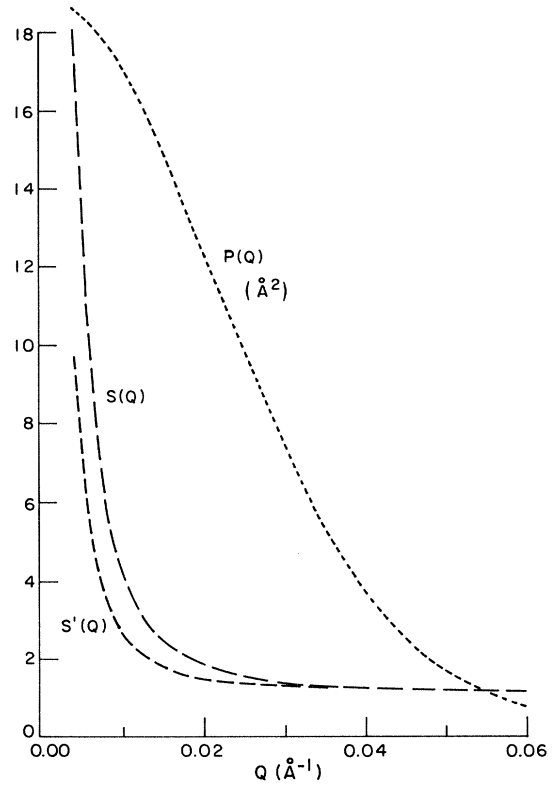

FIG. 5. Individual components contributing to the calculation of the $\phi=0.0746$ fitted curve of Fig. 3. Fitting parameters are $\bar{R}=46.0$ Å, $z=9.80$, $\Delta\rho=5.86\times10^{-6}$ Å^{-2}, $\xi=601$ Å, $\chi_T=116$.

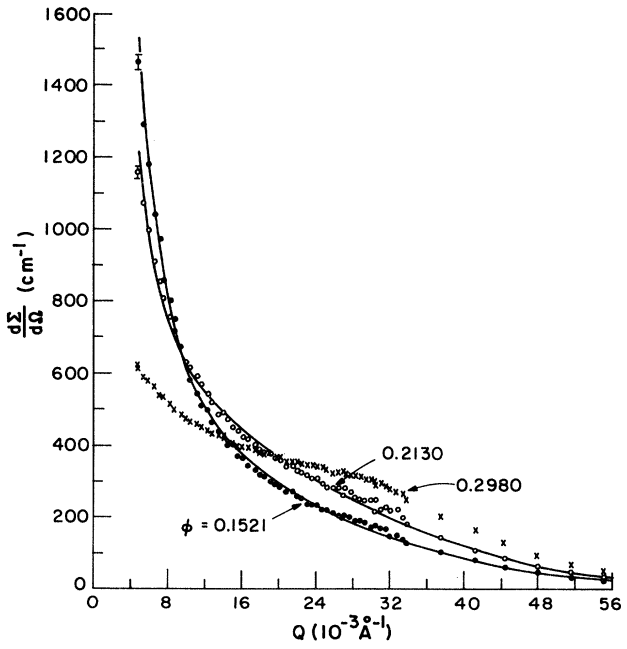

FIG. 4. SANS spectra at 39.7 °C for three volume fractions ϕ: 0.1521 (●), 0.2130 (○), 0.2980 (×). Solid curves represent best fits to $\phi=0.1521$ and 0.2130 data using OZ model for the structure factor. Spectrum for $\phi=0.2980$ could not be fitted.

are observing a dispersion of water droplets in a sea of oil. The measured $\Delta\rho$ is slightly below that for pure water and oil because of the penetration of AOT head groups into the water pool. To further substantiate the droplet picture, one also sees that the mean water core radius $\bar{R}$ and polydispersity p remain approximately constant for all volume fractions investigated at a given temperature. There is some evidence that the mean droplet size is only a weakly decreasing function of temperature, while the polydispersity weakly increases with temperature.

The OZ correlation length of critical fluctuations and zero-angle structure factor (which is proportional to the intensity of long-wavelength fluctuations) are depicted as a function of temperature and dilution in Fig. 7. The curves peak in the neighborhood of $\phi\cong0.08$, indicating the approximate critical concentration of the microemulsions. This is very close to the concentration of the 3-5-95 system, whose critical behavior has been previously investigated.[8–10] Light scattering studies by other workers[24] have indicated a peak in the scattered intensity for microemulsions containing water, sodium dodecyl sulfate, dodecane, and various alcohols. In all cases studied the maximum intensity was found to be between $\phi=0.06$ and 0.09, values very near our determination.

Figures 8 and 9 illustrate the effects of temperature on the critical scattering from a $\phi=0.0533$ microemulsion, along with the fitted curves obtained by using both the OZ and MSA models. Although the quality of the OZ fits is slightly better than those of the MSA, both structure fac-

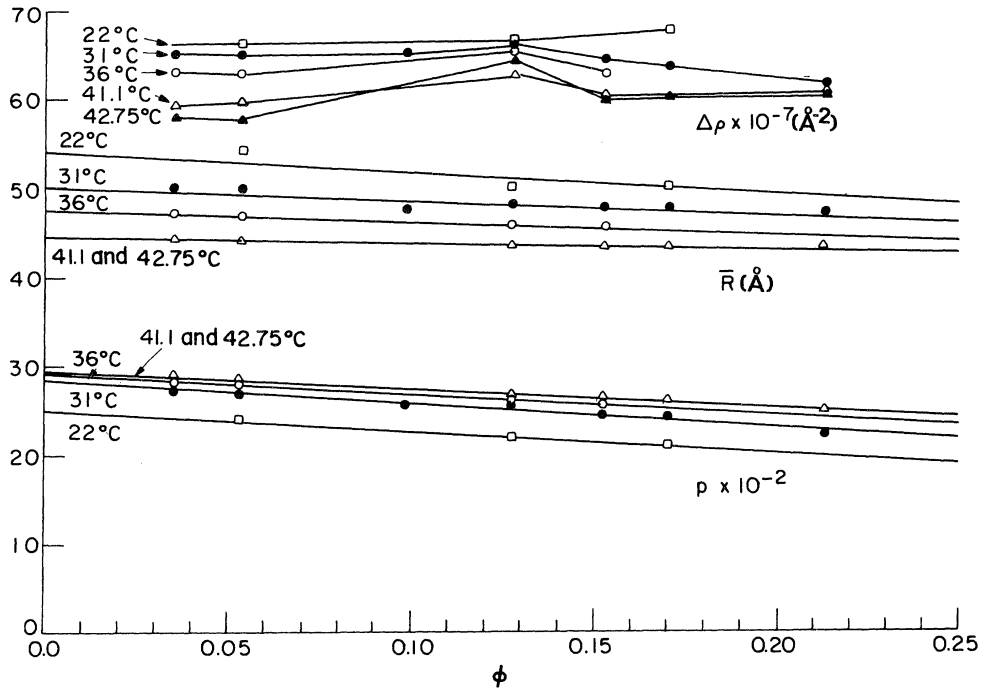

FIG. 6. Concentration dependence of mean water-core radius ($\bar{R}$), polydispersity (p), and contrast factor ($\Delta\rho$) at five temperatures: 22 °C (□), 31 °C (●), 36 °C (○), 41.1 °C (△), 42.75 °C (△ or ▲).

tors seem to model the data satisfactorily. However, agreement between experiment and the MSA model breaks down for volume fractions greater than about 0.07. This is not due to failure of the MSA to account for intermediate-Q structure, but because it fails to produce marked OZ asymptotic behavior at small Q. The MSA structure factors severely underestimate the forward scattering intensity. For those volume fractions where it is applicable, the MSA model has the inherent advantage of specifying the intra- and interparticle structure in a self-consistent way so that the structure factor properly accounts for the finite volume fraction of particles. This claim has been substantiated by Bendedouch and coworkers,[25] who successfully modeled micellar intra- and interparticle structure for a wide range of lithium dodecyl sulfate concentrations in aqueous solution. Figure 10 illustrates the MSA structure factors used to obtain the fitted curves of Fig. 9. The marked oscillatory behavior of the structure factors at intermediate Q become attenuated by the polydispersity factor $\beta(Q)$ used to obtain the best fits.

As shown in Table I, the values of the particle parameters $\bar{R}$, p, and $\Delta\rho$, found by fitting the SANS data from low concentration microemulsions with the MSA model, are very close to those found by applying the OZ model. The computed thickness δ of the surfactant-tail layer is

TABLE I. Temperature dependence of microemulsion droplet parameters determined by fitting spectra to MSA model for low values of volume fraction ϕ. (The values in parentheses were computed with the OZ model.)

	$\phi=0.0355$				$\phi=0.0533$					
T (°C)	31.0	36.0	41.1	42.75	31.0	36.0	39.4	41.1	42.5	42.75
$\Delta\rho$ (10^{-6} Å^{-2})	6.74 (6.52)	6.71 (6.31)	6.69 (5.94)	6.61 (5.81)	6.84 (6.51)	6.83 (6.29)	6.81 (6.00)	6.76 (5.97)	6.71 (5.77)	6.69 (5.75)
$\bar{R}$ (Å)	49.8 (50.0)	47.6 (47.2)	46.5 (44.3)	46.8 (44.3)	49.9 (49.8)	48.0 (46.8)	46.5 (44.0)	46.8 (44.1)	47.5 (44.0)	47.6 (43.9)
p	0.31 (0.27)	0.33 (0.28)	0.34 (0.29)	0.34 (0.29)	0.32 (0.27)	0.33 (0.28)	0.34 (0.29)	0.34 (0.29)	0.34 (0.28)	0.34 (0.28)
σ (Å)	125.4	121.2	119.0	119.8	126.2	122.4	119.2	120.0	121.4	121.6
δ (Å)	8.3	8.1	7.9	7.9	8.4	8.1	7.9	8.0	8.0	8.0
$\bar{N}$	546 (540)	504 (484)	484 (428)	491 (427)	551 (535)	514 (474)	485 (421)	491 (423)	505 (420)	507 (418)

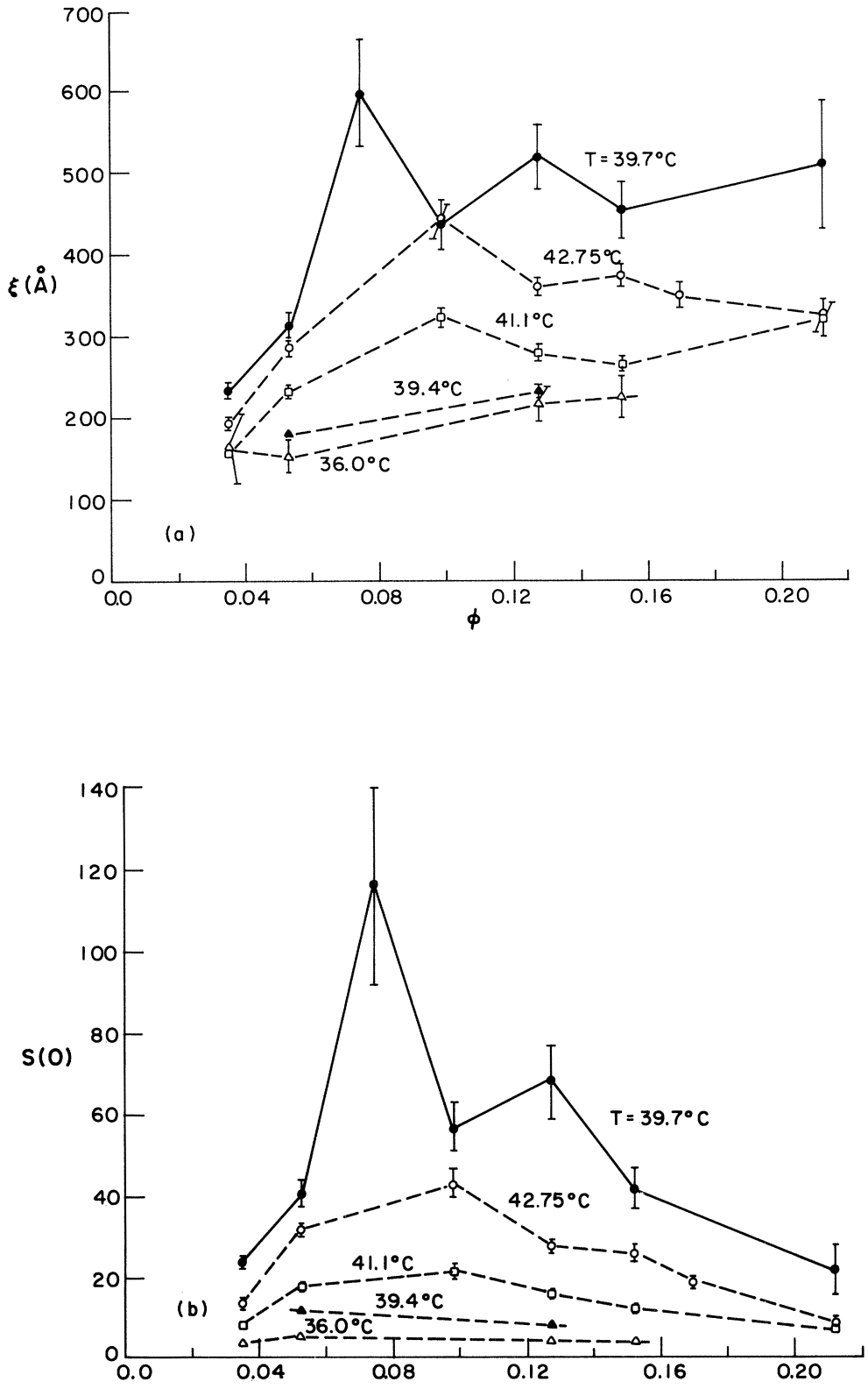

FIG. 7. Concentration dependence of the critical parameters for five temperatures T: 36°C (△), 39.4°C (▲), 41.1°C (□), 42.75°C (○), 39.7°C (●). (The $T = 39.7$°C parameters were extracted from microemulsions containing batch B surfactant, which produce lower cloud-point temperatures than the microemulsions with batch A surfactant used for the other measurements.) (a) Correlation length ξ. (b) Zero-angle structure factor $S(0)$.

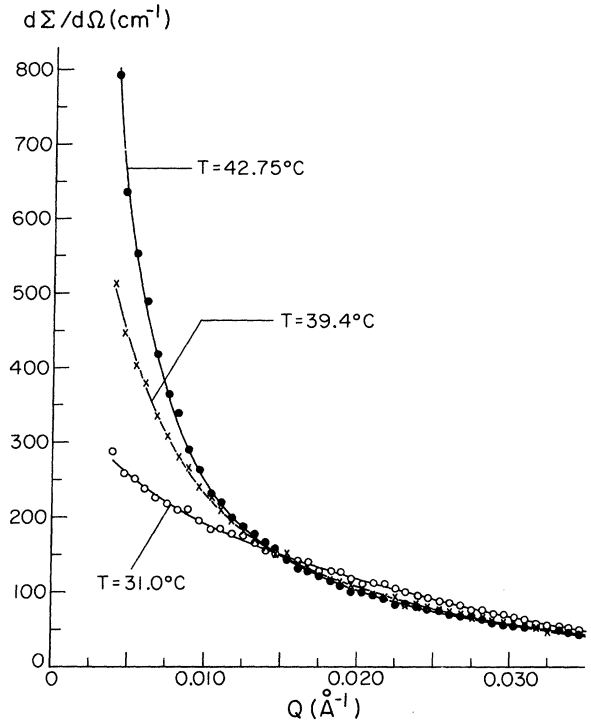

FIG. 8. SANS spectra for a $\phi=0.0533$ volume fraction microemulsion at three temperatures T: 31 °C (○), 39.4 °C (×), 42.75 °C (●). Solid curves are best fits to data using OZ model.

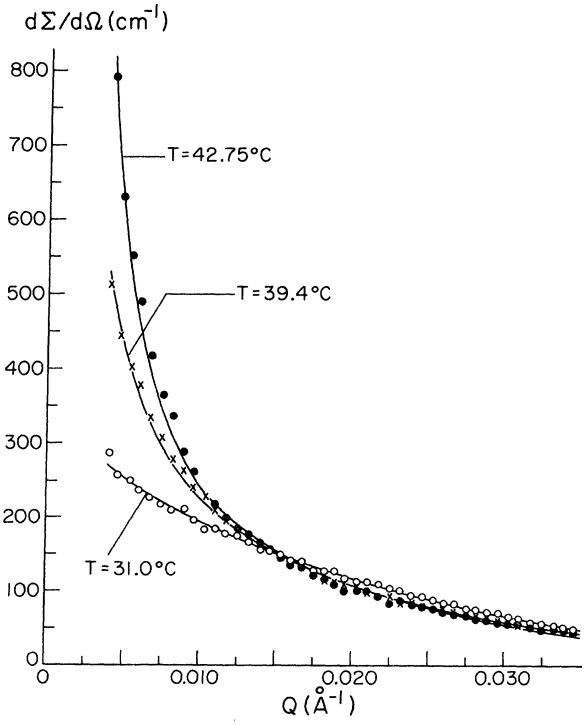

FIG. 9. Same spectra as in Fig. 8. Solid curves are best fits to data using MSA model.

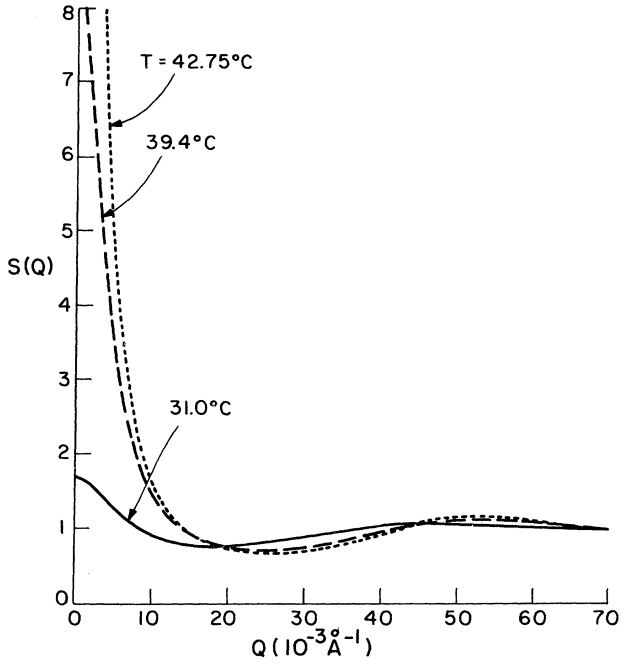

FIG. 10. MSA structure factors used in computing the fitted curves of Fig. 9.

approximately constant at 8 Å. Since the extended alkyl chain length for AOT (Ref. 26) is 9 Å, our result is in agreement with the claim that the water core is coated with a monolayer of surfactant molecules. In addition, Table I shows the results of estimating the mean aggregation number $\bar{N}$ of surfactant molecules per droplet using the expression

$$\bar{N}=4\pi\langle R^2\rangle/a_H=4\pi\left[\frac{z+2}{z+1}\right]\bar{R}^2/a_H\ , \tag{44}$$

where a_H is assumed to be constant at 62.5 Å^2 (see Sec. III).

The temperature dependence of the parameters k and γe^{-k}, which specify the interaction potential between a pair of droplets, is shown in Fig. 11. It appears that the interaction parameters do not depend strongly on the microemulsion concentration, at least not for the low volume fractions that could be fitted with the MSA. However, the marked increase of k and γe^{-k} with temperature indicates that the range of interaction decreases and the depth of the contact potential increases with temperature. The strength of the interaction can be measured by numerically computing B_2, the attractive portion of the second virial coefficient for the osmotic pressure, using the relation

$$B_2\sim-\int_1^\infty\{\exp[-U(x)/k_BT]-1\}x^2dx\ , \tag{45}$$

with $U(x)/k_BT$ given by Eq. (37). The measured values of k and γe^{-k} indicate that the magnitude of B_2 increases sixfold upon raising the temperature from 30 °C to 43 °C. This is evidence that the critical phenomenon is driven by the strength of the interparticle attraction, which is ex-

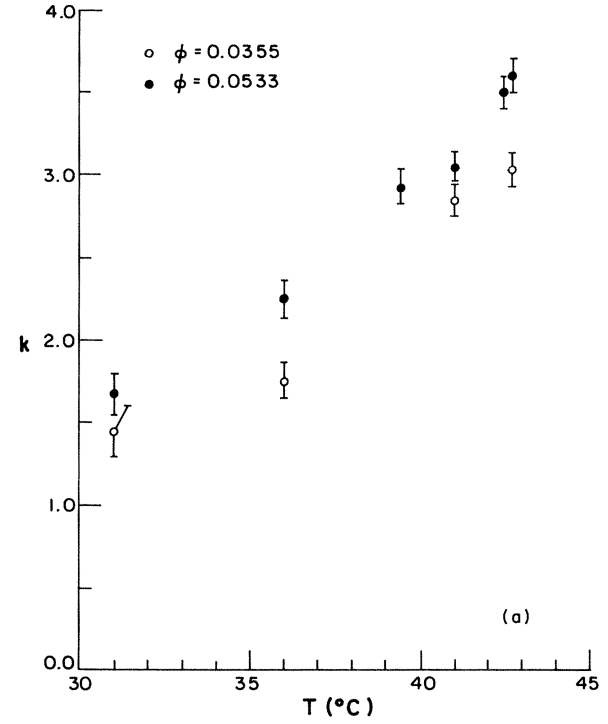

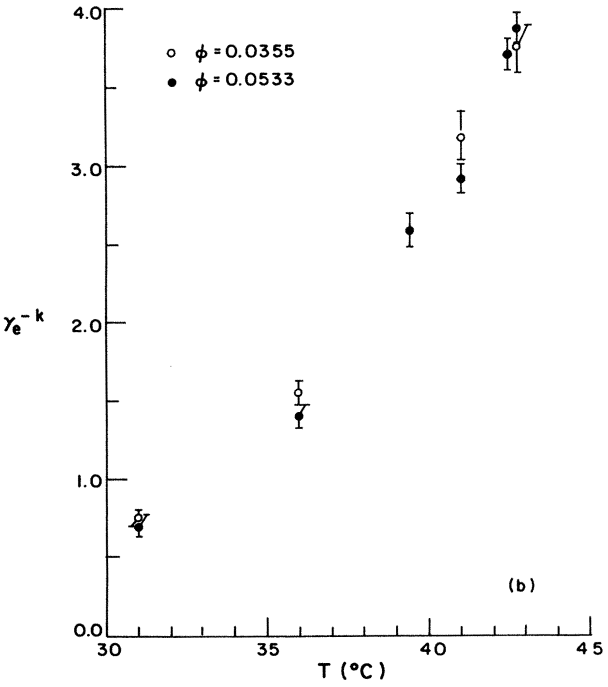

FIG. 11. Temperature dependence of the parameters describing the attractive portion of the interparticle potential for low values of the volume fraction ϕ. (a) Inverse range constant k. (b) Depth of contact potential γe^{-k}.

pected to increase with temperature for a system having a lower consolute point.

B. Phase separation study

Figure 12 shows the SANS spectra from the resultant upper and lower portions of the phase-separated $\phi=0.0746$ microemulsion at 41.3 °C. The solid curves are the best fits to the data using the OZ model. The spectra are shown on a semilog scale to emphasize the excellent quality of the fits over the extended range of Q. The agreement is typical of all the fitted spectra performed in our studies.

The values of the fitting parameters (see Fig. 12 caption) show that the droplet size and polydispersity are approximately the same ($\bar{R}=44$–45 Å, $p=0.29$–0.32) for both the upper and lower phase. As proposed by Safran and Turkevich,[27] this is evidence that the bending energy of the surfactant interface is much larger than either k_BT or the interdroplet interaction energy. When this bending energy is large, it is predicted that the coexisting phases should consist of a high and low density of droplets with identical radii, analogous to a binary mixture phase separation.

Since ϕ_{D_2O} is not known *a priori* for each of the individual phases, the n_p's cannot be computed from Eq. (35). As a result, the contrast factor $\Delta\rho$ is also unknown for both the upper and lower phase. However, by applying the expression for the zero-angle scattering cross section using Eq. (15), it can be shown that the volume fraction of water in either phase is given by

$$\phi_{D_2O}=\frac{\left.\frac{d\Sigma(\vec{Q})}{d\Omega}\right|_{\vec{Q}=0}}{\frac{4\pi}{3}\frac{\langle R^6\rangle}{\langle R^3\rangle}}\frac{1}{1+\chi_T\frac{\langle R^3\rangle^2}{\langle R^6\rangle}}\frac{1}{(\Delta\rho)^2}\,. \tag{46}$$

On the right-hand side, $\Delta\rho$ is the only parameter not directly measurable from the fit. That is, the volume fractions in the upper and lower phases, denoted by $\phi^U_{D_2O}$ and $\phi^L_{D_2O}$, can be expressed in terms of the unknown value of $\Delta\rho$, which one can assume to be the same for both phases. One can now write the volume conservation equation for the total volume fraction of water in the system $\phi^T_{D_2O}$ as

$$\phi^T_{D_2O}=(\phi^U_{D_2O}V^U+\phi^L_{D_2O}V^L)/(V^U+V^L)\,, \tag{47}$$

where V^U and V^L are the volumes of the upper and lower phases, respectively. The value of $\phi^T_{D_2O}$ in our phase separation study is 0.0487. Equations (46) and (47) can be combined to solve for the contrast factor, giving $\Delta\rho=5.75\times10^{-6}$ Å^{-2}. The individual volume fractions of water $\phi^U_{D_2O}$ and $\phi^L_{D_2O}$ can now be computed from Eq. (46). Since the droplet size is approximately the same in both phases, it is reasonable to extract the total volume fractions ϕ^U and ϕ^L by assuming that $\phi^U/\phi^U_{D_2O}=\phi^L/\phi^L_{D_2O}=\phi^T/\phi^T_{D_2O}=1.531$. The results of this calculation give $\phi^L=0.193\pm0.008$ and $\phi^U=0.024\pm0.002$. Figure 2 shows that these computed concentrations compare favorably with the coexistence curve determined by light

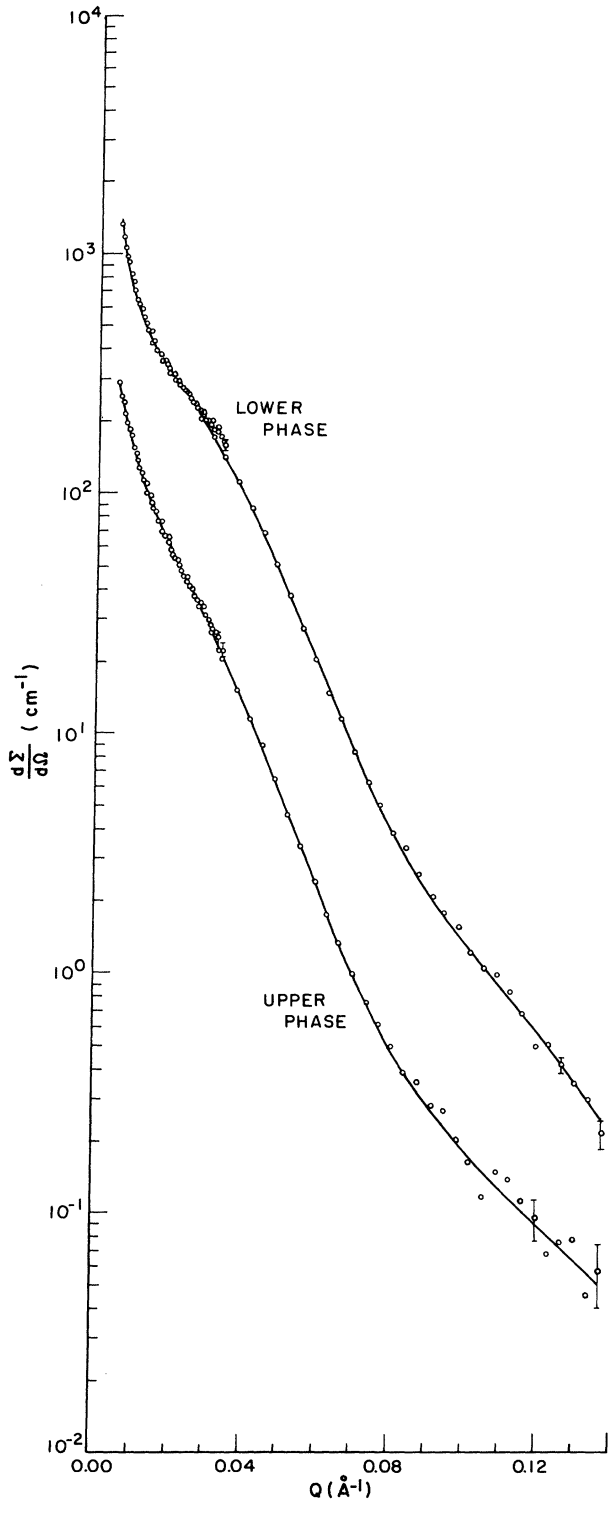

FIG. 12. SANS spectra from the upper and lower phases of a phase-separated microemulsion having an initial volume fraction of 0.0746. The solid curves are the best fits using the OZ model. Fitted parameters for upper phase are $z=8.62$, $\bar{R}=44.8$ Å, $\xi=196$ Å, $\chi_T=17.2$. For the lower phase $z=10.88$, $\bar{R}=44.0$ Å, $\xi=445$ Å, $\chi_T=31.9$.

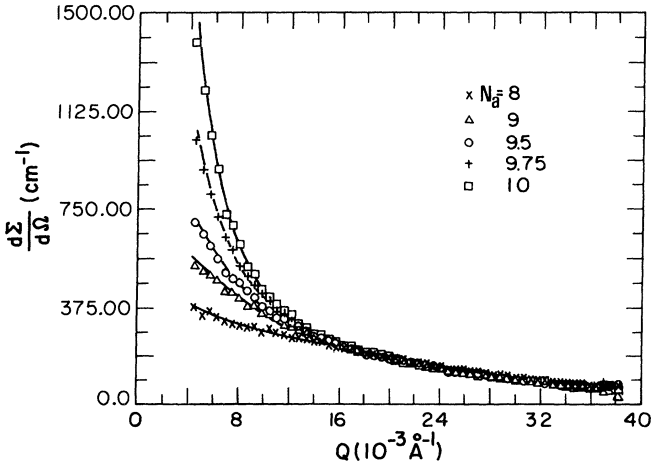

FIG. 13. Effect of varying the solvent alkane number N_a on the scattering from a 0.10 volume fraction microemulsion at 31.8 °C. Solid curves are best fits to data using the OZ model.

scattering, further substantiating the claim that ϕ is an appropriate order parameter for the critical phenomenon. Note that the determination of ϕ^L and ϕ^U hinged upon our knowledge of $d\Sigma(0)/d\Omega$ in Eq. (46). Since it is a straightforward matter to measure absolute cross sections in a SANS experiment, it appears that SANS is an ideal technique for measuring the coexistence curve at a fixed $[D_2O]/[AOT]$ ratio.

C. Alkane-number study

The SANS spectra of $\phi=0.10$ microemulsions at 38.1 °C are illustrated in Fig. 13 for five different values of the alkane number N_a. The alkane number dependence of the critical scattering is qualitatively very similar to the temperature dependence shown in Fig. 8. A striking feature of the data is that the spectra coincide for $Q>0.016$ Å^{-1}. Since the intensity in this Q region is primarily determined by particle scattering, this is strong evidence that the droplet size is unaltered by an approach to the critical point.

The OZ fitted curves are indicated by the solid lines in Fig. 13. For all the curves, the particle parameters are $\bar{R}=47.4$ Å and $p=0.28$. The increasing range and amplitude of the critical fluctuations as a function of N_a are plotted in Fig. 14. Roux *et al.*[28] have shown that the depth of the interaction potential between droplets in certain quaternary microemulsion systems is proportional to the difference between the molecular densities in the surfactant layer and the oil continuum. Their measurements suggest that this density difference increases with the molecular volume (v_{oil}) of the oil component, which may signify that the interaction strength depends on how difficult it is for the oil molecule to penetrate the surfactant layer. One should also notice, however, that the volume per carbon in the oil, i.e., v_{oil}/N_a, is a decreasing function of the alkane number. As a result the difference between the volume per carbon in the surfactant-tail layer and that in the oil increases as one goes from $N_a=8$ to 10. This may cause the strength of attraction to increase as the carbon number increases.

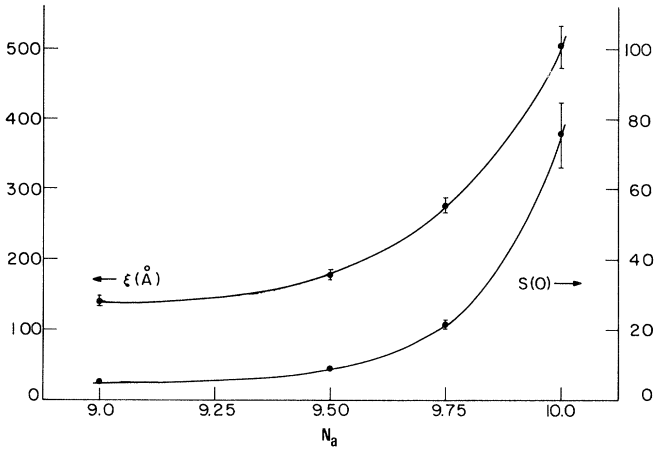

FIG. 14. Alkane-number dependence of the critical parameters ξ and $S(0)$ for a 0.10 volume fraction microemulsion at 38.1 °C.

VII. CONCLUSIONS

Small-angle neutron scattering measurments have been carried out over an extensive Q range capable of probing both the critical and particle scattering regimes. Two models, one phenomenological and the other microscopic, were used to analyze the data. The following set of conclusions has been drawn from such analyses.

The droplet model is well established for single-phase W/O microemulsions up to a volume fraction of about 15 vol. %. The basic structure of the droplets does not change as the temperature is raised toward the critical point.

The shape of the droplet is spherical, having a water core of radius 45—50 Å coated with an 8-Å monolayer of surfactant tails. The polydispersity of the droplets is between 25% and 35%. The SANS contrast factor $\Delta\rho$, determined to be $(6.3\pm0.5)\times10^{-6}$ Å^{-2}, corresponds to the difference in scattering-length density between the oil and water. Thus neutron scattering is caused by small water droplets dispersed in the continuous oil medium.

The phase separation experiment established that an appropriate order parameter for the critical phenomenon is the volume fraction ϕ of the droplets. The critical volume fraction is about 0.08. Our previous study[10] showed that the exponents γ and ν, which describe the divergences of the osmotic compressibility and correlation length of fluctuations, resemble those of a critical binary mixture. Thus our analysis is consistent with the picture that the critical scattering is caused by increased correlations between droplets near the critical point. This does not imply that the droplets form permanent aggregates, but rather that they form transient clusters leading to large fluctuations in the droplet number density.

The existence of a lower consolute point can be understood to be due to an increased strength of attraction between droplets as the temperature is raised. The increase in attraction can also be achieved by raising the alkane number of the oil solvent.

The upper and lower phase microemulsions contain well-defined W/O droplets, with the respective volume fractions given by the coexistence curve measured by light scattering. The droplet sizes and polydispersities in the upper and lower phases are nearly identical.

Above $\phi\cong0.20$ the validity of the droplet model begins to break down and a new structure appears to set in. This conclusion is also indicated from recent measurements performed on high concentration microemulsions represented by points $M1$—$M4$ on the ternary phase diagram of Fig. 1. SANS measurements on these compositions, along with some O/W microemulsions (points $W1$—$W3$), will be the subject of a future report.

ACKNOWLEDGMENTS

We acknowledge the staff of the National Center for Small-Angle Scattering Research (NCSASR) at the Oak Ridge National Laboratory for their generous allocations of spectrometer time, making this extensive set of measurments possible within a reasonable amount of time. We would also like to thank Oak Ridge Associated Universities for financing the trips to NCSASR. This research was supported by the National Science Foundation and the Exxon Research and Engineering Company. Financial support for the primary author during this work was provided by the Thompson Memorial Fellowship awarded by the Nuclear Engineering Department at the Massachusetts Institute of Technology.

APPENDIX: MULTIPLE SCATTERING AND TRANSMISSION MEASUREMENTS NEAR THE CRITICAL POINT

The calculations in this section demonstrate, in an approximate way, that the effects of multiple scattering can be neglected for microemulsions that exhibit small-angle critical scattering. In addition, the transmission of thermal neutrons through such samples is approximately independent of temperature and solvent carbon number. In the arguments to follow, we primarily consider the coherent small-angle scattering. Other contributions to the beam attenuation such as incoherent scattering and absorption only appear as a trivial attenuation factor when computing the effects of multiple scattering, as will be shown. Even though the measured transmission of our samples is close to 52%, which implies a large amount of scattering, numerical integration of the small-angle scattering intensities shows that most of the attenuation originates from the incoherent scattering of the hydrogen-rich solvent.

To discuss multiple scattering, we follow the formalism put forth by Schelten and Schmatz.[29] Define $H_1(\vec{Q})=D\,d\Sigma(\vec{Q})/d\Omega$ as the single-scattering probability, where D is the sample thickness and $d\Sigma(\vec{Q})/d\Omega$ is the differential cross section per unit volume. In principle, one would have to scatter from an infinitesimally thin sample to measure $d\Sigma(\vec{Q})/d\Omega$. In a real scattering experiment, however, one measures the quantity $d\Sigma^*(\vec{Q})/d\Omega$, which may include contributions from multiple scattering. The measured scattering probability is $H(Q)=D\,d\Sigma^*(\vec{Q})/d\Omega$.

The two scattering probabilities can be related through the transforms

$$h_1(r)=2\pi\int_0^\infty J_0(Qr)H_1(Q)Q\,dQ \tag{A1}$$

$$h(r)=2\pi\int_0^\infty J_0(Qr)H(Q)Q\,dQ\ , \tag{A2}$$

and inverse transforms

$$H_1(Q)=\frac{1}{2\pi}\int_0^\infty J_0(Qr)h_1(r)r\,dr \tag{A3}$$

$$H(Q)=\frac{1}{2\pi}\int_0^\infty J_0(Qr)h(r)r\,dr\ , \tag{A4}$$

by the relationship

$$h(r)=\mathcal{T}k_0^2\{\exp[h_1(r)/k_0^2]-1\}\ , \tag{A5}$$

where $k_0=2\pi/\lambda$ is the wave number of the incident radiation and $\mathcal{T}$ is the total transmission of the sample. The transmission can be written as

$$\mathcal{T}=\mathcal{T}'\cdot\mathcal{T}_{\rm SAS}\ , \tag{A6}$$

where $\mathcal{T}_{\rm SAS}$ is the coherent small-angle scattering contribution to the transmission and $\mathcal{T}'$ is the component of transmission due to absorption and any other types of scattering. $\mathcal{T}_{\rm SAS}$ is given by

$$\mathcal{T}_{\rm SAS}=1-\int_{4\pi}H(Q)d\Omega\ . \tag{A7}$$

Since $Q=k_0\theta$ for small-angle scattering through an angle θ, Eqs. (A2) and (A5)–(A7) give

$$\mathcal{T}=\mathcal{T}'[1-h(0)/k_0^2]=\frac{\mathcal{T}'}{1+\mathcal{T}'\{\exp[h_1(0)/k_0^2]-1\}}\ . \tag{A8}$$

Now consider the model case of critical scattering from particles with size much smaller than the interparticle correlation length ξ. An approximate expression for the single-scattering probability is the Ornstein-Zernike form

$$H_1(Q)=\frac{H_1(0)}{1+Q^2\xi^2}\ . \tag{A9}$$

Clearly, we have neglected the Gaussian-type rolloff of the scattering intensity at large Q. However, the fact that the total scattering is overestimated means that our conclusions regarding multiple scattering will be conservative ones.

First let us consider how the transmission $\mathcal{T}$ of such a sample changes as the temperature approaches the critical point. From Eq. (A8) one sees that if $\mathcal{T}'$ is approximately temperature independent, the total transmission only depends on $h_1(0)$. Substituting Eq. (A9) into Eq. (A1) gives

$$h_1(0)=\frac{\pi H_1(0)}{\xi^2}\ln[1+(Q\xi)^2_{\rm max}]\ , \tag{A10}$$

where we have truncated the upper limit of integration at a reasonably large $(Q\xi)_{\rm max}$, say about 40. Since $H_1(0)\sim\xi^2$ for a critical system, $h_1(0)$ is approximately independent of ξ. This means that, for a truly critical system, $h_1(0)$ is independent of temperature and one should expect very little change in both the transmission and the integrated intensity measured over the two-dimensional detector as temperature is raised toward the critical point. This conclusion is substantiated by observing that the integrated count rate over the detector is almost independent of temperature in the critical region.

Experimentally one measures the transmission at NCSASR by placing a strong scatterer (glassy carbon) into the beam path between the sample and the detector, causing the count rate of the detector to be proportional to the transmitted flux. In this way, the beamstop need not be moved to measure transmission. However, as the critical point is approached, the scattering becomes sufficiently forward peaked to also be scattered by the carbon into the detector. As a result, the measured value of $\mathcal{T}$ seems to rise as the temperature is raised toward the critical point. This is clearly a false result. However, because we expect that $\mathcal{T}$ should not change significantly, one can bypass this problem by simply measuring $\mathcal{T}$ relatively far from the critical temperature and assuming this transmission value for those points close to the phase boundary.

To estimate the effects of multiple scattering on the Q dependence of the scattered intensity, we numerically computed the scattering probability $\int_{4\pi}D[d\Sigma^*(\vec{Q})/d\Omega]d\Omega$ for a spectrum collected very close to the critical temperature. The scattering probability was $h(0)/k_0^2=0.062$. Because this number is so much less than unity, Eq. (A5) shows that $h_1(0)/k_0^2\approx h(0)/k_0^2$. In addition, since $h_1(r)$ is a decreasing function of r, one is justified in considering only the leading terms in the expansion of Eq. (A5) for $h(r)$. So

$$h(r)=\mathcal{T}h_1(r)+\frac{\mathcal{T}}{2k_0^2}[h_1(r)]^2\ . \tag{A11}$$

Substituting this into Eq. (A4) gives

$$H(Q)=\mathcal{T}H_1(Q)+\frac{\mathcal{T}}{4\pi k_0^2}\int_0^\infty J_0(Qr)[h_1(r)]^2r\,dr\ . \tag{A12}$$

Using our expression for $H_1(Q)$, i.e., Eq. (A9), $h_1(r)$ can be computed[30] with Eq. (A1) to be

$$h_1(r)=\frac{2\pi H_1(0)}{\xi^2}\int_0^\infty\frac{x}{1+x^2}J_0\left[\frac{r}{\xi}x\right]dx=\frac{2\pi H_1(0)}{\xi^2}K_0(r/\xi)\ , \tag{A13}$$

where $K_0(x)$ is the zeroth-order modified Bessel function of the second kind. Inserting into Eq. (A12) gives

$$H(Q)=\mathcal{T}H_1(Q)+\mathcal{T}\frac{\pi}{k_0^2\xi^2}[H_1(0)]^2g(Q\xi)\ , \tag{A14}$$

where

$$g(Q\xi)=\int_0^\infty J_0(Q\xi x)K_0^2(x)x\,dx\ . \tag{A15}$$

The integral $g(Q\xi)$ can be evaluated explicitly[31] to obtain a final expression relating $H(Q)$ to $H_1(Q)$:

$$\frac{H(Q)}{\mathcal{T}H_1(0)}=(1+4\alpha^2)^{-1}+\frac{\pi H_1(0)}{4k_0^2\xi^2}\alpha^{-1}(1+\alpha^2)^{-1/2}\times\ln\left[\frac{(1+\alpha^2)^{1/2}+\alpha}{(1+\alpha^2)^{1/2}-\alpha}\right], \quad \text{(A16)}$$

where $\alpha=Q\xi/2$. Again, since $H_1(0)/\xi^2$ is a temperature-independent constant, the functional form of the result only depends on the dimensionless parameter $Q\xi$ for a given microemulsion composition. Note, however, that there is the temperature-dependent scaling factor $\mathcal{T}H_1(0)$. For a 3-5-95 microemulsion at 0.7 °C below the cloud point, it was previously found[10] that $\xi\approx 920$ Å and $H_1(0)\approx 2160$. The results of numerically evaluating Eq. (A16) show that $H(Q)$ and $\mathcal{T}H_1(Q)$ never differ by more than 3% at any value of $\alpha<20$. Based on these approximate calculations one can conclude, therefore, that the effects of multiple scattering are sufficiently small to be ignored for the microemulsions under study.

[1]M. Dvolaitzky, M. Goyot, M. Laguës, J. P. Le Pesant, R. Ober, C. Sauterey, and C. Taupin, J. Chem. Phys. 69, 3279 (1978).

[2]C. Cabos and P. Delord, J. Appl. Crystallogr. 12, 502 (1979).

[3]R. A. Day, B. H. Robinson, J. H. R. Clarke, and J. V. Doherty, J. Chem. Soc., Faraday Trans. 1 75, 132 (1979).

[4]M. Zulauf and H. F. Eicke, J. Phys. Chem. 83, 480 (1979).

[5]A. M. Cazabat, D. Langevin, and A. Ponchelon, J. Colloid Interface Sci. 73, 1 (1980).

[6]D. J. Cebula, R. H. Ottewill, J. Ralston, and P. Pusey, J. Chem. Soc., Faraday Trans. 1 77, 2585 (1981).

[7]M. Dvolaitzky, M. Laguës, J. P. Le Pesant, R. Ober, C. Sauterey, and C. Taupin, J. Phys. Chem. 84, 1532 (1980).

[8]J. S. Huang and M. W. Kim, Phys. Rev. Lett. 47, 1462 (1981).

[9]J. S. Huang and M. W. Kim, *Proceedings of the Society of Petroleum Engineers—DOE Third Joint Symposium on Enhanced Oil Recovery, Tulsa, 1982* (Society of Petroleum Engineers of the American Society of Mechanical Engineers, Dallas, 1982), p. 901.

[10]M. Kotlarchyk, S. H. Chen, and J. S. Huang, Phys. Rev. A 28, 508 (1983).

[11]S. H. Chen, C. C. Lai, J. Rouch, and P. Tartaglia, Phys. Rev. A 27, 1086 (1983).

[12]M. Kotlarchyk, S. H. Chen, and J. S. Huang, J. Phys. Chem. 86, 3273 (1982).

[13]We follow the procedure previously given by M. Kotlarchyk and S. H. Chen, J. Chem. Phys. 79, 2461 (1983).

[14]See, for example, B. Jacrot, Rep. Prog. Phys. 39, 911 (1976).

[15]T. Assih, F. Larché, and P. Delord, J. Colloid Interface Sci. 89, 35 (1982).

[16]D. Bendedouch, S. H. Chen, and W. C. Koehler, J. Phys. Chem. 87, 153 (1983).

[17]This is to insure that the critical micelle concentration of AOT in decane is maintained.

[18]The specific volume of AOT in oil (xylene) solutions has been measured to be 0.8789 cm^3/g, which is very close to the specific volume of dry AOT. See P. Ekwall, L. Mandell, and K. Fontell, J. Colloid Interface Sci. 33, 215 (1970).

[19]L. S. Ornstein and F. Zernike, Proc. Sect. Sci. K. Med. Akad. Wet. 17, 793 (1914).

[20]J. L. Lebowitz and J. K. Percus, Phys. Rev. 144, 251 (1966).

[21]J. P. Hansen and J. B. Hayter, Mol. Phys. 46, 651 (1982).

[22]J. B. Hayter and M. Zulauf, Colloid Polym. Sci. 260, 1023 (1982).

[23]J. B. Hayter and J. Penfold, Mol. Phys. 42, 109 (1981).

[24]G. Fourche, A. M. Belloco, and S. Brunetti, J. Colloid Interface Sci. 88, 302 (1982).

[25]D. Bendedouch, S. H. Chen, and W. C. Koehler, J. Phys. Chem. 87, 2621 (1983).

[26]D. Oakenfull, J. Chem. Soc., Faraday Trans. 1 76, 1875 (1980).

[27]S. A. Safran and L. A. Turkevich, Phys. Rev. Lett. 50, 1930 (1983).

[28]D. Roux, A. M. Bellocq, and P. Bothorel, in *Surfactants in Solution,* edited by K. L. Mittal and B. Lindman (Plenum, New York, 1983).

[29]J. Schelten and W. Schmatz, J. Appl. Crystallogr. 13, 385 (1980).

[30]*Handbook of Mathematical Functions With Formulas, Graphs, and Mathematical Tables,* edited by M. Abramowitz and I. A. Stegun (U.S. GPO, Washington, D.C., 1970), p. 488.

[31]I. S. Gradshteyn and I. M. Ryzhik, *Table of Integrals, Series, and Products* (Academic, London, 1980), p. 672.